Hindawi
Mobile Information Systems
Volume 2022, Article ID 5411119, 11 pages
https://doi.org/10.1155/2022/5411119

Research Article

Experimental Research on Span Direction Effect of Vortex-Induced Vibration of Bridge Main Girder Based on Symmetric Algorithm

Xiaochuan Cao and Yuhu Luo

School of Civil Engineering, Chongqing Jiaotong University, Chongqing 400074, China

Correspondence should be addressed to Xiaochuan Cao; cxiaoch@cqjtu.edu.cn

Received 23 May 2022; Revised 18 June 2022; Accepted 5 July 2022; Published 22 July 2022

Academic Editor: Shadi Aljawarneh

Nowadays, the research of digital geometry is gradually shifting from low-level geometric attributes to high-level semantic attributes. The symmetry of the 3D geometric model is an important bridge between the underlying geometric information of the related model and the high-level semantic information. Symmetry analysis is an important issue in geometric processing. Bridge safety is a major issue related to the national economy and people's livelihood. Therefore, the bridge structure health monitoring system is becoming a research focus in academic and technical circles. Wireless sensor network has been widely used in bridge health monitoring system due to its convenient installation, low maintenance cost, and flexible deployment. This article summarizes the existing bridge health monitoring system based on wireless sensor network. In the bridge control system of wireless sensor network, the basic principles and typical methods are introduced in turn, and the key technologies in the system are analyzed in combination with several specific examples. Finally, the existing problems and future research directions of the existing system are summarized. During the operation stage, vortex-induced resonance often occurs below the wind speed. The vortex excitation force of the main actuator along the axis of the bridge is related to the actual wind field and its own structural vibration. This article briefly introduces typical cases and control measures of vortex-induced vibration of long-span bridges, and summarizes the current research status of vortex-induced vibration of bridge main girder structures. At the same time, the vortex-induced vibration of bridge girder is experimentally studied by using symmetrical algorithm.

1. Introduction

Since the 1970s in modern times, with the further rapid development and wide application of various sensors and 3D model system builders and other technologies, based on the symmetric semantic algorithm, we can analyze the basic structure of the model semantically, and symmetrically apply it to 3D solid geometric model, morphological view description, mode view segmentation, simulation, and view editing [1]. This paper analyzes the symmetry vector detection of the important research topic of the three-dimensional geometric model in the data analysis application field [2]. Based on the highest-level three-dimensional geometric model attributes under the three-dimensional geometric model, this paper analyzes the inherent symmetry of the three-dimensional model [3]. The most important thing is analyze the local symmetry of the local bottom layer of the model with higher complexity, and the local intrinsic symmetry of many different aspects, such as large noise and lack of complex data processing [4]. With the continuous advancement of 3D geometric model batch acquisition and model modeling processing technology, 3D geometric models have gradually received more and more international attention and attention [5]. The structural analysis and modeling processing of 3D geometric models, especially in the high-level 3D Geometric model processing has gradually become a hot topic, among which symmetry algorithm is widely regarded as a very critical basic structure processing information in 3D geometric models, and it is an important basis for how to perform high-level 3D geometric model

processing and modeling work [6]. This article will introduce the main research and development background of the subject in detail from two main perspectives: the semantic synthesis analysis of the three-dimensional geometric model and the important application significance of the symmetry inspection algorithm in the research of the semantic synthesis analysis of the geometric model [7]. The wireless sensor center network node is a new type of sensor node network, which is integrated by a large-scale wireless sensor network node with strong visual information perception realization ability, calculation and analysis ability, and Internet data communication processing ability [8]. With the rapid progress and continuous development of national modern detection and monitoring equipment and wireless sensor node network communication technology, some large-scale bridges have been prepared to deploy wired sensor networks during their normal construction and wiring process, which will be able to target the operation of each bridge in the future. Real-time monitoring is carried out, but the monitoring system has a high cost in the process of wiring installation and maintenance [9]. Special construction sites are difficult to wire and are vulnerable to harsh construction environmental conditions, and the distance of the data transmitted will also be affected by the traditional wiring process [10]. Due to the large length constraint, the wireless sensor node network can have several major advantages such as easy wiring installation of monitoring equipment, low maintenance cost and low cost, and flexible equipment deployment [11]. It can well solve the problems that the monitoring system may encounter in actual engineering applications. The large amount of data collected through real-time monitoring and collection of various wireless sensor node networks can be used for real-time comprehensive information processing and data analysis, and timely and accurately grasp the normal monitoring operation and operation status of each bridge in the safe production, use and engineering operation management of modern large-scale bridges provide basic guarantees [12]. With some revolutionary innovations in bridge science and engineering technology, people's technical level in the construction of various bridges has also been greatly improved. The main girder structure of modern bridges has many structural shapes. Some of them directly adopt streamlined auxiliary sections with good aerodynamic separation properties and are relatively stable. The main girder structures involved in these main girders are likely to directly cause a large amount of flow through the main girder subsidiary sections, resulting in tension adhesion and vibration separation. Its working principle can be roughly divided into structural measures and aerodynamic measures.

2. Related Work

The literature mainly introduces the symmetry point pair reflecting the potential symmetry in the model, which is to accurately define the two vertices corresponding to them to have similar symmetric geometric point pair properties according to the basic concept of symmetry, in order to quickly and effectively remove inappropriate corresponding point pairs to reduce the computational complexity of the model [13]. First of all, it is necessary to analyze and judge the relative point pair attributes according to the symmetric point pair attributes near the two corresponding vertices, construct, and give a basic symmetry constraint. And to prescribe conditions, and quickly exclude pairs of points that do not meet any basic constraint conditions at the same time [14]. The monitoring and analysis system mentioned in the literature mainly uses various types of sensor equipment to perform real-time monitoring and analysis, to obtain some relevant information about the internal environmental stress stimulus of the bridge and the stress response of the bridge structure, and then fully adopt wireless signal processing and analysis in the bridge design stage [15]. Some indexes related to the bridge state are analyzed and extracted by using data processor and other technologies. In the bridge design stage, the stress damage data in the bridge structure are fully used for dynamic identification, and the technology is used to comprehensively evaluate the health management state of relevant bridges. In order to effectively ensure the safe and normal operation of the bridge and provide a more scientific evaluation basis for its future maintenance work, the literature mainly introduces in detail the application modules that some sensor communication nodes need to consume information energy [16]. With the continuous improvement of the current communication integrated circuit design and manufacturing process, the energy consumption of multiple functional modules such as sensor node modules and signal processors has gradually become very small, and nearly 80% of communication nodes are concentrated on the energy consumption of multiple functional modules such as wireless communication. Therefore, in order to effectively reduce the energy data sent and received by each communication node, the wireless communication sensor adopts a duty-cycling processing mechanism in the field of international network communication and real-time processing of the related information energy in the network [17]. The wireless monitoring system introduced in the literature uses various types of sensors for real-time monitoring to obtain various bridge environmental stimuli and structural responses, and then uses signal analysis and data processing techniques to automatically extract the operating status indicators of the bridge [18]. The spontaneous excitation force directly determines the convergent vector value of the motion spanwise correlation coefficient of the spanwise vortex excitation force of the main beam section, while the forced excitation force directly affects the spanwise vortex excitation force of the main beam section. The greater the compulsive force, the greater the correlation length of the spanwise-related effects, and the slower the attenuation speed of the spanwise coefficient of the aerodynamic vortex [19]. Through design and in-depth analysis, the literature studies the main girder node segment structure model of the bridge model, and carries out the main girder wind tunnel test of the bridge synchronization main girder vibration measurement and the wind pressure test of the main bridge node segment structure model, and obtains the bridge main girder segment structure in the locked response interval of the main beam vortex vibration under different angles of

wind tunnel attack; the correlation coefficient of the vortex excitation force on the section of the main beam section is much larger than that of the main beam static state.

3. Symmetrical Algorithms and Research on Key Technologies of Sensors

3.1. Symmetry Analysis Based on Symmetric Point Pairs. Symmetrical point pair refers to two symmetrical vertices on a model. The spatial distance relationship formula (1) of the symmetrical shape symmetrical radial function between the two symmetrical vertices X and X' is shown as follows:

$$d_{SDDE}(X, X\prime) = \left\| E_{SDE}(X) - E_{SDE}(X\prime)_{L_2} \right\|, \tag{1}$$

where d is the vertex distance of a vertex shape radial function, E is the length description definition expression of a vertex distance X of the shape radial function.

When two pairs of points meet the condition of a certain distance constraint, or when the degree of asymmetry is much smaller than the threshold of a certain distance, it can collectively reflect a kind of intrinsic symmetry in the model, due to the degree of this asymmetry. And the distance between the two points where the point pair is located is related to each other, so we use a relative threshold, where max is the highest value of the geodetic distance between all vertices, and the condition of the distance constraint can also be written by (2).

$$\begin{aligned} &RD((X, X\prime), (Y, Y\prime)): d((X, X\prime), (Y, Y\prime)) \\ &= \max \left\| d_G(X, Y) - d_G(X\prime, Y\prime) \right\|. \end{aligned} \tag{2}$$

For the point pair $\{X, X'\}$ on the model M, the support point pair is not unique, but there may be many support point pairs. The set of all the support point pairs of the point pair $\{X, X'\}$ is

$$\Pi_{(X,X\prime)} = \{(X_i, X_i') | X_i \in M. \tag{3}$$

In this model, a set of support point pairs is often not exactly symmetrical, and the degree of asymmetry can be measured by an average relationship between the degree of asymmetry between two support point pairs.

$$d_{\text{symmetry}}\left(\Pi_{(X,X\prime)}\right) = \frac{\sum_{(X_i,X_i')\in\Pi_{(X,X')}} d(X, X\prime), (X_i, X_i'))}{\left|\Pi_{(X,X\prime)}\right|}. \tag{4}$$

where $d_{\text{Symmetry}}(\Pi_{(X,X\prime)})$ is the asymmetry degree of the point pair $\{X, X'\}$ supported by the point pair set.

$$\begin{aligned} S_{ij} &= S\left(X_i, X_j\right) \\ &= \inf_{f\in F:\ f(X_i)=X_j} D_f(X, f(X)), \end{aligned} \tag{5}$$

where f is an intrinsic combination transformation on the vertex model, and X is a vertex in the neighborhood of the combined vertex model X_i on the vertex model, where

$$D_f\left(X_i, X_j\right) = d_{\text{symmetry}}\left(\Pi_{\left(X_i, x_j\right)}\right). \tag{6}$$

Get the matrix $\widetilde{C}$:

$$\widetilde{C}_i = e^{-\left(S_{ij}/\sigma \text{SCM} \times d_{max}\right)^2}. \tag{7}$$

The symmetric unit number simplified matrix algorithm used in this article is mainly

$$C = D^{-1/2}\widetilde{C}D^{-1/2}. \tag{8}$$

In the distance between symmetric vertices, it is pointed out that under the precise symmetric physical conditions, the corresponding analysis matrix of symmetric solution is shown in Figure 1. In order to fully facilitate our real-time observation, the relationship system matrix of symmetric solution correspondence has been rearranged to rearrange all the symmetric vertices in the same track and their corresponding track rows and columns. By solving symmetrically, the values of nonzero characteristic points and symmetric eigenvectors of the relation matrix can be obtained directly, and the precise connotation and symmetry of the whole model can be obtained.

After the linear relationship vertex matrix decomposition corresponding to the symmetrical vertices is embedded in the spectrum curve diffusion space, the diffusion distance of the symmetrical vertex decomposition can also be simply regarded as a symmetry of a symmetrically diffused spectrum model on an overall model structure. The diffusion distance, the entire diffusion model can also be simply regarded as the overall structure of a diffusion graph.

According to this design feature, it can be used to design and construct the distance between the symmetrical decompositions between different vertices. The higher the symmetric gradient optimization degree, the smaller the distance between the symmetrical decompositions between the vertices. First, embed the vector relational expression corresponding to the symmetry into the spectral space in matrix form:

$$E^t(X_i) = \left(\lambda_1^t \Psi_1(X_i), \ldots, \lambda_n^t \Psi_n(X_i)\right). \tag{9}$$

The Euclidean distance is used to measure the degree of symmetry of the vertex, and the symmetry decomposition distance of the vertex is

$$\begin{aligned} d_{SER}'\left(X_i, X_j\right) &= ||E^t(X_i) - E^t\left(X_j\right)||^2 \\ &= \sum_{k=1}^{n} \lambda_k^t |\Psi_k(X_i) - \Psi_k\left(X_j\right)|^2. \end{aligned} \tag{10}$$

Since the feature distance values of the first few items are significantly larger than the feature distance values of the other models, when t is used to take a larger feature value, the later feature distance values of the symmetric model can be directly ignored, and the decomposition distance of the symmetric model is only the same as the previous one. The feature distance values of several items are related, and the feature distance values of the first few items directly correspond to the symmetry of the model, so the symmetric

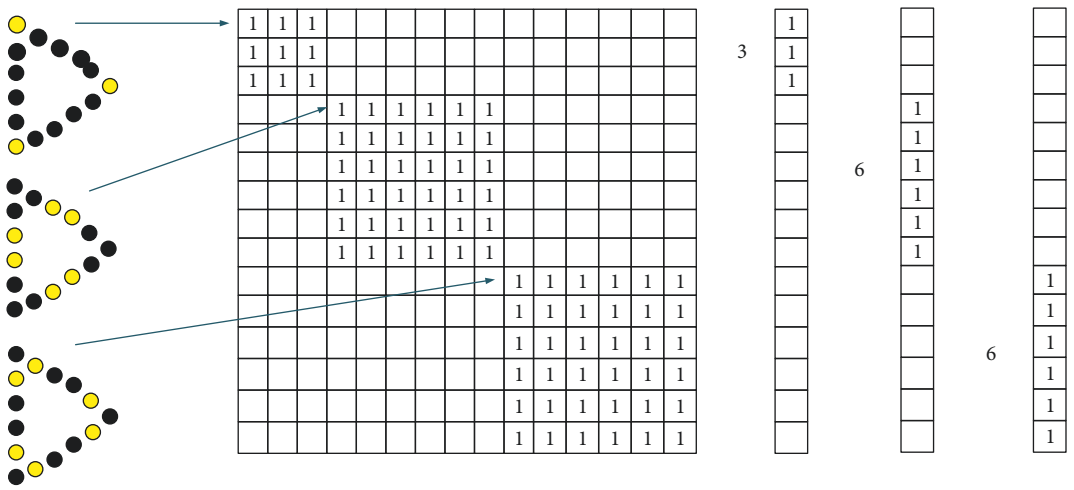

Figure 1: Schematic diagram of symmetric correspondence matrix and eigenvalue eigenvectors.

model decomposition distance value can be used to measure the model symmetry between the feature vertices of the same model.

Based on the above discussion, the thermocore descriptor itself has geometric vertex properties that are invariant to equidistant symmetric transformations. Therefore, we can even apply it to calculate and analyze the degree of symmetry transformation between the geometric vertices. The difference between the two geometric vertices x and y on the same mathematical model, and the difference between the geometric vertex attributes within a certain range can be used in a certain time area and the calculation integral of the thermal core description operator attribute difference is applied to measure it numerically.

$$\left(\int_{t_1}^{t_2}\left|S_{HKS}(x,t)-S_{HKS}(y,t)\right|^2 \mathrm{d}t\right)^{1/2} = \left(\int_{t_1}^{t_2}\left|k_t(x,x)-k_t(y,y)\right|^2 \mathrm{d}t\right)^{1/2}. \tag{11}$$

Then, the size of the gap between the two geometric vertices x and y in a certain adjacent domain can be expressed by the transformation of formula (12):

$$d_{HKS_{[t_1,t_2]}}(x,y)=\left(\int_{t_1}^{t_2}\left|\frac{k_t(x,x)}{\int_M k_t(x,\mathrm{x})}-\frac{k_t(y,\mathrm{y})}{\int_M k_t(y,y)}\right|^2 \mathrm{d}t\right)^{1/2}. \tag{12}$$

Calculate the thermocore descriptor:

$$d_{HKS_{[t_1,t_2]}}(x,y)=\left(\sum_{t_0=t_1}^{n}\left|\frac{k_t(x,x)}{k_t(x,\mathrm{x})}-\frac{k_t(y,\mathrm{y})}{\int_M k_t(y,y)}\right|^2\right)^{1/2}. \tag{13}$$

Since the thermocore descriptor only contains the information of the local vertex geometric model data set near a vertex, it does not contain the geometric displacement spatial relationship between the geometric part of the vertex model and the vertex as a whole.

$$d_{SYM_{[t_1,t_2]}}(x,y)=d_{HKS_{[t_1,t_2]}}(x,y)\times d_G(x,y). \tag{14}$$

An asymmetry degree matrix can be established at different times, each item of which is relative to the degree of asymmetry between each vertex on the model.

$$S_{[t_1,t_2]_{ij}}=d_{SYM_{[t_1,t_2]}}\left(x_i,x_j\right). \tag{15}$$

The model covered by the asymmetric matrix is a descriptor.

3.2. Key Technologies of Sensor Networks. As shown in Figure 2, the SPEM management module and CS optimization management module are added to the framework of the system structure health detection and monitoring system proposed in this article. These two optimization modules are configured between the finite element management model and the node management deployment type module. It is used to correctly select the reasonable health check points and data addresses. The SPEM optimization module mainly relies on the position information of the two analog quantities of the network structure, the data write set of the position information of the target node to be measured, and the number of positions of the target node that needs to be measured on-site to filter and calculate the most optimized measurement in a detection project. The specific location of the target node and the FIM simulation value of the location of each measurement node; the CS optimization detection module mainly relies on the original SPEM optimization module to write and output the position data, combined with the structural characteristics of the wireless measurement sensor detection network and the needs of specific practical applications, Recombinate and design a set of target detection point position data to be selected and a set of candidate detection points and node magnitudes required by the application. Multiple iterations between the detection modules can directly obtain a final target detection point.

The various node deployment methods mentioned above all have certain technical limitations: SPEM is mainly suitable for finite element analysis methods, mainly from the broad

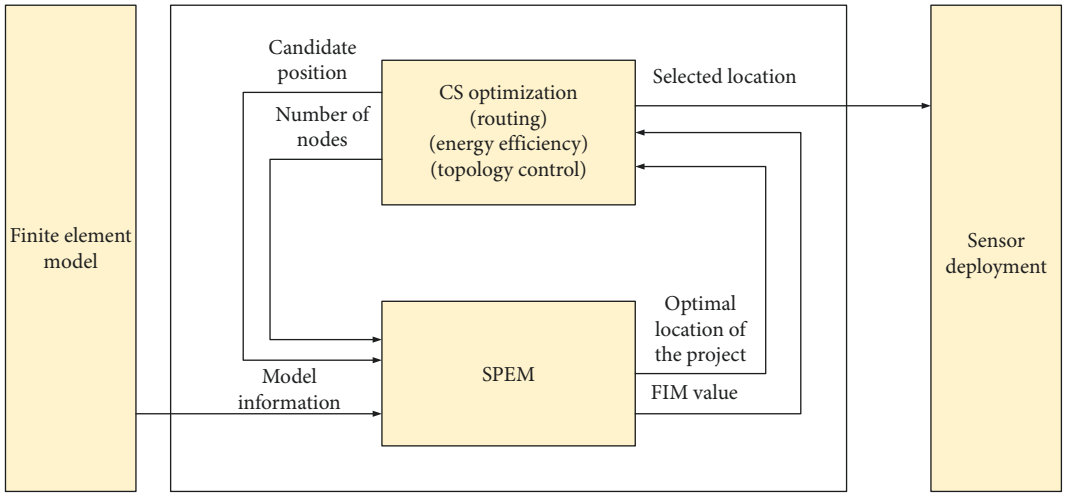

Figure 2: Node deployment method using EFI.

technical direction of structural health monitoring, taking into account the deployment of nodes, and passing experiments are performed on tower bridges and other buildings to obtain and verify their effects, but there are still certain differences between these bridges and their structures.

The sensor processing node first performs a subliminal numerical quantification judgment on the vibration radio frequency signal compression data threshold obtained by each sampler through collection and analysis, and saves and processes the vibration signal compression data whose data reaches a certain frequency threshold value. The data undergoes threshold quantization, subthreshold value judgment segmentation, run-length signal encoding, and encapsulation, and finally sends it to the base station node. When the network data collection manager located at the base station node needs to retrieve and review the original compressed data or when deleting the remaining data details, the compression information is sent by the base station node for secondary compression according to the original data compression sequence stored in the flash.

After each node receives the data packet of the previous node, it merges its own information and data, and then uses the same method to send it to the next node, and finally all the data reaches the node at the other end, in order to effectively balance the energy of each node, each time the data is transmitted according to the last transmission direction of a different node.

4. Experimental Study on the Spanwise Effect of Vortex-Induced Vibration of the Main Girder of a 4 Long-Span Bridge

4.1. Test Model and Working Conditions. In order to conduct in-depth discussion on the correlation between the spanwise directions of different main beam vortex excitation force models, 5 rows of pressure tapping holes are designed and arranged at different positions of the vortex excitation force spanning directions. The schematic design of the pressure tapping whole layout is shown in Figure 3. The new electromechanical pressure transmission scanning solenoid valve detection system of PSI Corporation of the United States is used, and the stability performance of the electronic pressure transmission is tested. When the model is undergoing pressure test, an electronic automatic pressure test scanning valve is directly placed inside the test model. The test hydraulic scanning valve is connected to each other with a hole equipped with a pressure measuring tube on the main surface of the model. The scanning valve and the computer are connected to each other again. It is connected through the use of the computer's pressure controller operation to directly and automatically complete the pressure test. The vibration frequency of each sampling of the electronic pressure scanning valve can be directly set to 331 Hz, and the duration of sampling at each wind speed can be directly set to 20 s.

The results of this experiment failed to propose in-depth the torsional vortex motion effect, but only considering the observation of a vertical vortex motion effect that the structure may produce, the motion equation is actually defined as (16):

$$m\frac{\partial^2 z}{\partial t^2} + C_z\frac{\partial z}{\partial t} + EI\frac{\partial^4 z}{\partial x^4} - H\frac{\partial^2 z}{\partial x^2} = -L(z, \varnothing, \mathrm{t}). \tag{16}$$

The vertical bending frequency of the brace model is expressed as:

$$f_z = \frac{1}{2L}\sqrt{\frac{H}{m} + \left(\frac{\pi}{L}\right)^2\frac{EI}{m}}. \tag{17}$$

The main advantage of the brace model is that the use of the steel wire rope's transverse bending tensile stiffness can effectively provide the brace model's own lateral motion stiffness, and for the brace forming model itself, the lateral bending tensile stiffness of the outer garment is relative to the brace model itself The contribution is very small and can be ignored. Then, (17) can be simplified as shown in (18):

$$f_z = \frac{1}{2L}\sqrt{\frac{H}{m}}. \tag{18}$$

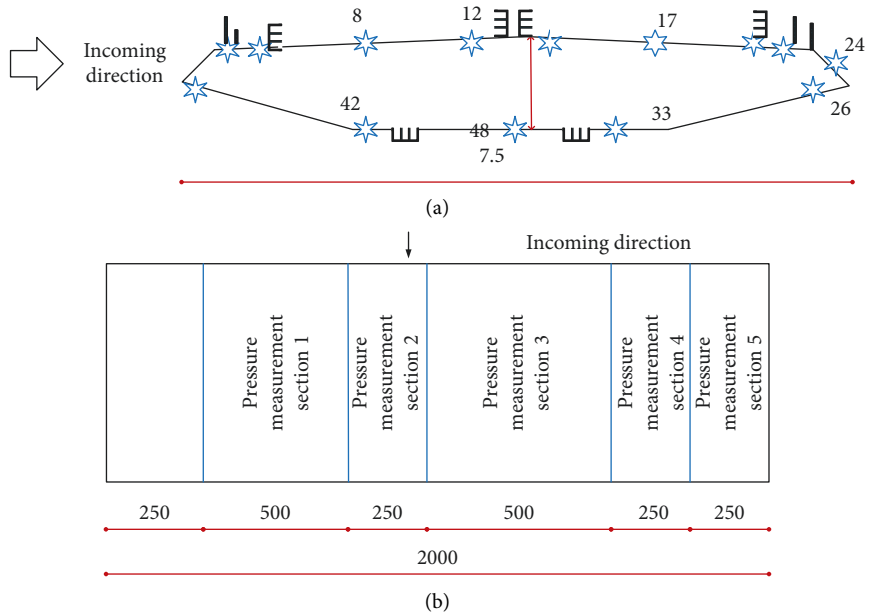

Figure 3: Schematic diagram of pressure measuring hole layout. (a) Layout of pressure measuring holes on each pressure measuring section. (b) Layout plan of the pressure measurement section along the span.

The brace model needs to follow the following similar principles during the design process, such as geometry, inertial parameters, elasticity, and damping parameters. Due to the limitation of the size and dimensions of the wind tunnel, the viscosity parameters failed to meet the requirements. Unlike the full-bridge aeroelastic model, the brace model can be designed without considering the influence on the gravity parameters.

The correlation coefficient is a unified measurement standard used to measure the complexity of the relationship between linear variables. The absolute value ranges of the variables that need to be used are [−1, 1], and the absolute value range of the correlation coefficient is the larger the value, the higher the complexity of this linear correlation may become. When its absolute value is 0, it is called irrelevant, and when its absolute value is 1, it is called complete correlation. The correlation coefficient of the two function variables of X and Y can be expressed clearly by the (19):

$$R_{XY} = \frac{\sum (X - \overline{X})(Y - \overline{Y})}{\sqrt{\sum (X - \overline{X})^2 \sum (Y - \overline{Y})^2}}. \tag{19}$$

Replace the two variables of X and Y in the above formula with different aerodynamic parameter variables of different pressure aerodynamic detection system sections, that is, we can directly analyze and obtain the spanwise-related aerodynamics of different aerodynamic forces between various pressure sections. Coefficient, namely,

$$R_{c_i}(\delta/D) = \frac{\cot[C_i(\delta/D)]}{\mathrm{Var}[C_i]}. \tag{20}$$

Existing experimental studies have provided an approximate formula for the correlation coefficient of the aerodynamic span of the bluff body section:

$$R_{C_i}(\delta/D) = \exp\left[-C_i \frac{\delta}{D}\right]. \tag{21}$$

The correlation size of the aerodynamic parameter c_i can also be defined by the span length:

$$\frac{L_i}{D} = \int_0^{\infty} R_{C_i}\left(\frac{\delta}{D}\right) \mathrm{d}\left(\frac{\delta}{D}\right) = \frac{1}{C_i}. \tag{22}$$

The spanwise correlation of the vibration of the structure is often greater than that of its static state, so when the structure vibrates, the (21) becomes the (23):

$$R_{C_i}\left(s_j, \frac{\delta}{D}\right) = \exp\left[-C_i(s_j)\frac{\delta}{D}\right]. \tag{23}$$

where s is a component statistical parameter related to the displacement of the location. That is to say, (23) also considers the spanwise correlation along with the change between spanwise spacing and vibration amplitude.

$$R_{C_i}\left(s_j, \frac{\delta}{D}\right) = \exp\left[-C_i(s_j)\left(\frac{\delta}{D}\right)^p\right]. \tag{24}$$

Regardless of whether it is for the vertical or torsional vortex state, the researchers have proposed a method. The ratios of the corresponding lift parameter-related system index and the attenuation fitting parameter between the vertical state and the torsional vortex state are expressed as:

$$C_i = \frac{0.01578}{0.02694 + (h/D)}, \qquad C_i = \frac{0.00551}{0.01058 + \alpha}. \tag{25}$$

Table 1: Comparison table of design parameters between the brace model and the segment model.

Parameter name	Symbol	Unit	Real bridge value	Design scale value	Segment model value		Stretch model value	
					Design value	Realized value	Design value	Realized value
Length of main beam	L	m	—	1/80	2	2	6	6
Width of main beam	B	m	39	1/80	0.5125	0.3251	0.3254	0.2415
Height of main beam	H	m	3.425	1/80	0.120	0.201	0.130	0.022
Equivalent mass	m_{eq}	Kg/m	28047	$1/80^2$	4.4521	4.2762	4.2145	4.2153
Vertical bending fundamental frequency	f_v	Hz	0.1425	20	5.685	4.52	5.654	3.210
Vertical bending damping ratio	ξ_v	%	0.2	1	0.6	0.215	0.4	0.526
Wind speed ratio	—	—	—	—	4	4.85	4	7.51

Table 2: Dynamic parameters of the first 3 modes of the brace model.

Mode shape	Frequency (Hz)			Damping (%)
	Theoretical value	Measured value	Error (%)	Measured value
First order vertical frequency	2.152	3.120	1.52	0.532
Second order vertical frequency	5.845	5.652	−1.35	0.854
Third order vertical frequency	8.685	8.669	−0.62	1.263

In this regard, it is proposed to use equation (26) to fit the spanwise correlation coefficient of the vortex excitation force during structural vortex vibration:

$$R_{c_i}\left(\frac{\delta}{D}\right) = (1 - d_i)\exp\left[-C_i\frac{\delta}{D}\right] + d_i. \tag{26}$$

Performing a pressure integration on the pressure of different materials in each row of sections can obtain the three-component force measurement coefficients on the sections of different pressure measurement materials, the comprehensive calculation of the lift coefficient, and the torque pressure coefficient. The integral processing formula is shown in (27) and (28).

$$C_L(t) = \frac{\sum_{i=1}^{n} p_i(t)\cdot L_i\cdot\cos(\alpha_i)}{0.5pU^2B}, \tag{27}$$

$$C_M(t) = \frac{\sum_{i=1}^{n} p_i(t)\cdot L\cdot\mathrm{Sin}(\alpha_i)d_{iy} + \sum_{i=1}^{n} p_i(t)\cdot L_i\cdot\cos(\alpha_i)d_{ix}}{0.5pU^2B^2}. \tag{28}$$

4.2. Model Parameters and Test Conditions. The test section wind tunnel has a length of 15 m, a width of 8.5 m, and a height of 2 m. The wind speed control range of the test section is generally 0 ~ 14 m/s. It is an open large-scale test section. The tail wind tunnel can be directly used to simulate large-scale rainfall phenomena. The main design is suitable for large-span highway bridges, large-scale high-rise buildings, power transmission model simulation wind tunnel test, large-scale pollution diffusion process simulation, and large-scale wind and rain combined effect simulation wind tunnel test. In this paper, the main design application parameters of a bridge brace design model corresponding to the main design application parameters of the segment model are shown in Table 1.

The comparison results of the theoretical value and the actual measured value of the vertical bending dynamic characteristics of the brace model are shown in Table 2. The range of wind speed in the test section of the brace model is 0 ~ 6 m/s, and the range of Reynolds number is 0 ~ 3.0122 × 104.

In Table 3, the spanwise correlation of the vortex lift coefficient and the selected important representative wind speed in the vortex vibration interval are shown. The vortex vibration interval is set to +3 without the underlined angle of attack value in Table 3, and when the vortex vibration interval is underlined the angle of attack value is set to +5°.

According to the coefficient value of the aerodynamic spanwise correlation between discrete force breakpoints, the system model design is fitted to a different wind attack angle as shown in Figure 4, and different spanwise wind speed discrete points when vortex vibration occurs; the lift curve in which the spanwise lift coefficient changes with the spanwise spacing. Therefore, as shown in Figure 4, each lift curve is continuously improving. The necessary time course and performance of the nonzero lift measurement coefficient show a huge correlation of the spanwise movement distance, which will continue to increase with the spanwise movement distance. And gradually it is shown that it can gradually decay exponentially. The spanwise correlation of the space curve spacing of the same spanwise node in the first locking part is smaller than that of the other two wind speed control nodes; the amplitude lift coefficient of the second locking part at the end of the rising section is much larger than the maximum point of the amplitude in the first lock interval.

Table 4 shows a parameter value that is fitted by the numerical method of calculating the system using the correlation of the angle of attack between the discrete points.

In other words, the gradual increase in the motion threshold of the wind angle of attack is the main decisive

Table 3: Wind speed selection table for spanwise correlation analysis of lift coefficient during vortex vibration.

Vibration state	First lock	First lock	First lock	First lock	First lock	Second lock	Second lock
Description	Zone starting point	Area ascending section	Area maximum point	Descent section	Zone end point	Area ascending section	Area maximum point
Wind speed (m/s)	1.52	2.52	2.42	2.52	2.95	5.10	5.75
Vertical immeasurable	8.2451	11.2541	12.6253	12.7541	13.5423	24.2235	28.1542
Gang wind speed	9.1557	11.1524	12.1320	12.2512	12.7541	23.1142	28.1532
Vertical immeasurable	0.0101	0.0320	0.1202	0.2152	0.0001	0.0323	0.0215
Amplitude	0.1020	0.3320	0.1200	0.4155	0.0011	0.0521	0.1362

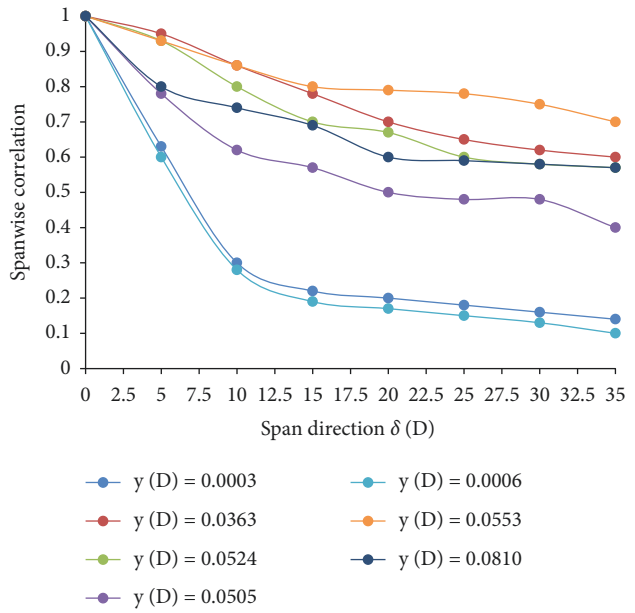

Figure 4: The spanwise correlation of lift coefficient varies with spanwise spacing during vortex vibration.

factor that directly leads to the spanwise motion correlation of the angle of attack.

4.3. Test Results and Analysis of Spanwise Effect of Vortex-Induced Vibration of Bridge Main Girder. Figure 5 shows the vertical dimensionless amplitude of the measurement points at the four positions of the +3° angle of attack as a function of the converted wind speed.

It can be seen from Figure 5 that the maximum amplitude of the first locking interval is much larger than that of the second locking interval.

Figure 6 shows the corresponding curves between the spanwise torque correlation coefficients and the time span spanwise correlation coefficients during the torsional wind vortex vibration between different spanwise wind speed points at different wind attack angles.

It can be clearly seen from Figure 6 that, generally speaking, the lifting torque coefficient corresponding to different wind speeds at various wind attack angles and the coefficient related to the spanwise direction change due to the increase of the spanwise spacing. With the acceleration of the wind attack angle, the final convergence value corresponding to the lift torque coefficient and the correlation coefficient will also increase overall, indicating that the wind attack angle is accelerated, which will lead to the acceleration of the self-excited force and the spread of the lift torque. The correlation coefficient has been greatly affected.

After the maximum detection value of the vortex vibration amplitude involved in various vertical vortex bending modes is converted through a normalized vibration model function calculation, the vortex amplitude of other selected detection points at their location can be directly obtained. The amplitude can be compared with the results in the actual vortex vibration test. Table 5 shows the actual estimated value of the vertical bending vortex amplitude value in the first stage and the measurement comparison of other test values. It can be clearly seen from Table 5 that the amplitude of the response of the vortex vibrator placed near the detection point at different detection positions should be roughly distributed according to the mode function.

Table 6 shows the comparison between the estimated value of the second-order vertical bending vortex amplitude value and the measured value. From Table 6, it can be seen that the different positions are roughly distributed according to the mode shape.

Table 7 shows the actual estimated value of the vertical bending vortex amplitude value in the third stage and the measurement comparison of the other test values. It can be seen from Table 7 that in the third test stage, the actual measurement error margin of the conversion test itself is relatively small, resulting in a large relative error between the converted value and the actual test value.

4.4. Application of Wireless Sensor Network in Bridge Health Monitoring. The application of wireless sensor network in bridge health monitoring can be seen: in actual engineering applications, it can be summarized as the following points.

(1) Selection and deployment of sensors

When selecting this type of sensor, it is necessary to determine its specific type and corresponding quantity according to the actual measurement situation and needs, and combined with the country's economic budget decision. Specifically, technical indicators such as measurement accuracy and measurement area range must be considered. Therefore, the deployment

Table 4: Fitting table of aerodynamic spanwise correlation parameters during vortex vibration.

Vibration state	First lock	First lock	First lock	First lock	First lock	Second lock	Second lock
Description	Zone starting point	Area ascending section	Area maximum point	Descent section	Zone end point	Area ascending section	Area maximum point
Fitting parameters	0.215	0.125	0.325	0.021	0.125	0.001	0.042
C_i	0.210	0.120	0.415	0.326	0.442	0.120	0.001
Fitting parameters	0.125	0.177	0.045	0.065	0.262	0.115	0.105
D_i	0.325	0.125	0.541	0.623	0.142	0.091	0.483
Obsessive-compulsive	5.262	21.142	21.324	12.023	4.523	8.521	9.241
Length $1/C_i$	5.021	36.102	36.132	18.524	5.865	6.652	7.021

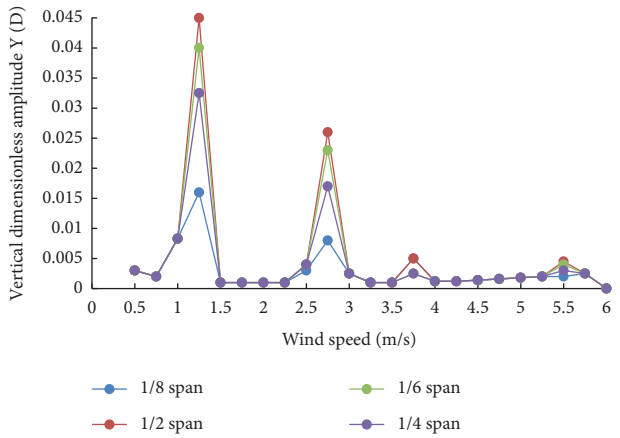

Figure 5: The vertical dimensionless amplitude of each measuring point varies with wind speed.

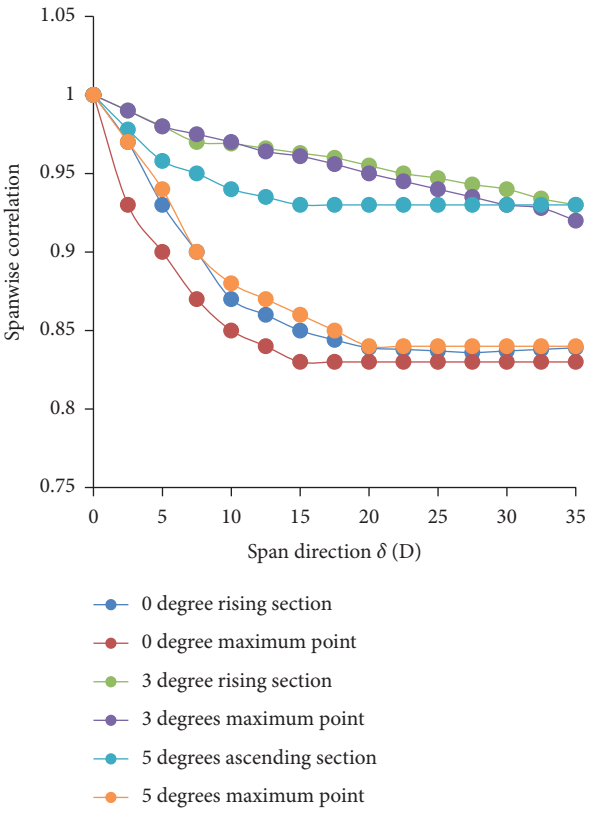

Figure 6: The spanwise correlation of torque coefficient varies with spanwise spacing during vortex vibration.

solution of sensor nodes is still a topic worthy of our in-depth exploration and research.

(2) Life of the health monitoring system

The service life of the health monitoring system mainly depends on the remaining energy of each node. Therefore, the energy efficiency of the node is also the first issue that we must fully consider in the process of designing the health monitoring system. Therefore, how to do this is for the bridge under the condition of normal operation of the health monitoring system, the energy of each node is used in a reasonable and targeted manner, and reliable energy signal collection and wireless charging technologies are used to compensate for the energy of the node in time. These technologies are worthy of our research and experimentation.

(3) Data storage and processing

The bridge health monitoring system generates a large amount of data on the network every day. If the information cannot be processed in a timely and effective manner, it will inevitably bring data disasters to the network. Therefore, on the one hand, for real-time collection and collection through sensors, data requires us to select appropriate algorithms for timely analysis and processing; on the other hand, we need to formulate reasonable data protection and storage strategies, and regularly and effectively remove excess resources from the entire database.

(4) The effect of structural damage recognition

Due to the incomplete and inaccurate measurement data and the limitations of the existing damage identification methods currently used, the practical application effect of structural damage identification is restricted, which directly affects the accuracy of the system evaluation results. Therefore, how to improve and increase the integrity of the detected data information database and the accuracy of the detection

Table 5: Comparison of the estimated and experimental values of the first-order vertical bending vortex amplitude.

Measuring point	Normalized coordinates	Normalized mode shape function	Test	Convert	Relatively error
	x/l	$\sin(n\pi x/l)$	Dimensionless vertical amplitude	Dimensionless vertical amplitude	
1/8	0.021	0.251	0.02415	0.01542	−5.65%
1/2	1.120	0.320	0.01253	—	—
1/6	0.524	0.452	0.12032	0.04512	0.35%
1/4	0.588	0.620	0.21530	0.12532	2.21%

Table 6: Comparison of estimated value and test value of second-order vertical bending vortex amplitude.

Measuring point	Normalized coordinates	Normalized mode shape function	Test	Convert	Relatively error
	x/l	$\sin(n\pi x/l)$	Vertical dimensionless amplitude	Vertical dimensionless amplitude	
1/8	0.214	0.532	0.01445	0.01622	4.55%
1/2	0.412	0.000	0.02135	0	—
1/6	0.523	−0.765	0.01523	0.12032	−8.35%
1/4	0.652	−1.010	0.12365	—	—

Table 7: Comparison of estimated value and experimental value of third-order vertical bending vortex amplitude.

Measuring point	Normalized coordinates	Normalized mode shape function	Test	Convert	Relatively error
	x/l	$\sin(n\pi x/l)$	Dimensionless vertical amplitude	Dimensionless vertical amplitude	
1/8	0.231	0.845	0.01021	0.02325	−11.14%
1/2	0.412	−1.021	0.02153	—	—
1/6	0.563	0.023	0.01532	0	—
1/4	0.625	0.652	0.02365	0.02032	35.65%

is the focus and direction that we need to further explore and research. On the other hand, we also need to actively explore and use new detected high sensitivity index technology to improve and enhance the effect of damage recognition.

5. Conclusion

This paper mainly researches and proposes a detection algorithm based on the local intrinsic symmetry of the model. This detection algorithm is not limited to the reflection symmetry of the local vertex of the symmetry detection. It is based on the three-dimensional geometric attributes near the local vertex of the model and the local symmetry decomposition between the local vertex of the distance relationship. Compared with the traditional manual detection and monitoring methods and modern wired network monitoring methods, wireless sensor networks are widely used in the field of bridge health monitoring and have certain advantages due to their simple installation, low maintenance cost, and flexible system deployment., The bridge structure health monitoring system based on wireless sensor network has become the focus of wide attention of academic circles and engineers at home and abroad. This article sorts out the wide application of wireless sensor network in bridge health monitoring system, and analyzes some of them in combination with some specific cases. Generally speaking, wireless sensor networks are currently widely used to monitor the bridges. There are still many difficulties. These problems are related to each other and hinder each other, which constitute the rich content of future research topics, but we can still be accurate. It is predicted that in the future, the bridge structure health monitoring system will play an increasingly important role in the management of bridges. The era of bridge digitalization is also quietly coming. In view of the problems of the vortex-induced vibration of the main shaft of long-span bridges, the use of two methods of synchronous vibration test and pressure test are adopted. The span-direction effect correlation test is carried out on the main beam segment model and the brace model under different wind attack angles. The response curve of the vortex-induced vibration lift response coefficient of the main bridge structure varying with the wind speed of the main girder was obtained. The bridge node wave band response model and the main girder tie section model were compared and analyzed. In the lift response to the vortex-induced vibration and the main girder, there is still a close correlation between the change of lift response coefficient and the spread direction for research. A dynamic identification method based on the system calculation model, a method for analyzing and identifying the excitation response of a rectangular vibration section of

the main beam, and an identification method for a streamlined main beam vortex-induced aerodynamic system were established. For the section, the response parameter calculation of the main beam vortex-induced vibration system and the comprehensive identification of the streamlined main beam vortex-induced aerodynamic system parameters were carried out, and the numerical comprehensive simulation of the method, the identification results, and the actual measurement results were combined for numerical comprehensive analysis and comparison. The application accuracy of the identification method in the actual calculation process is verified.

Data Availability

The data used to support the findings of this study are available from the corresponding author upon request.

Conflicts of Interest

The authors declare that they have no conflicts of interest.

References

[1] X. Fan, B. Zhou, and H. H. Wang, "Urban landscape ecological design and stereo vision based on 3D mesh simplification algorithm and artificial intelligence," *Neural Processing Letters*, vol. 53, no. 4, pp. 2421–2437, 2021.

[2] H. Santosa, F. Nur, and W. Adrian, "Management and enhancement of livable urban streetscape through the development of the 3D spatial multimedia system," *International Review for Spatial Planning and Sustainable Development*, vol. 9, no. 4, pp. 10–30, 2021.

[3] S. M. Cho, "Effects of digital elevation model in water quality modeling using geogrpahic information system," *International Journal of Internet, Broadcasting and Communication*, vol. 13, no. 2, pp. 14–19, 2021.

[4] M. Adil, M. Attique, M. M. Khan, J. Ali, A. Farouk, and H. Song, "Hopctp: a robust channel categorization data preservation scheme for industrial healthcare Internet of things," *IEEE Transactions on Industrial Informatics*, vol. 9, no. 3, p. 1, 2022.

[5] N. Tosa, P. Yunian, R. Nakatsu, A. Yamada, T. Suzuki, and K. Yamamoto, "3D modeling and 3D materialization of fluid art that occurs in very short time," in *Lecture Notes in Computer Science*, vol. 12523, pp. 409–421, Springer, Cham, Switzerland, 2020.

[6] D. A. Loaiza Carvajal, M. M. Morita, and G. M. Bilmes, "Virtual museums. captured reality and 3D modeling," *Journal of Cultural Heritage*, vol. 45, pp. 234–239, 2020.

[7] V. Di Pietra, E. Donadio, D. Picchi, L. Sambuelli, and A. Spanò, "Multi-source 3D models supporting ultrasonic test to investigate an Egyptian sculpture of the archaeological museum in b," *The International Archives of the Photogrammetry, Remote Sensing and Spatial Information Sciences*, vol. XLII-2/W3/W3, pp. 259–266, 2017.

[8] H. Abulkasim, A. Farouk, H. Alsuqaih, W. Hamdan, S. Hamad, and S. Ghose, "Improving the security of quantum key agreement protocols with single photon in both polarization and spatial-mode degrees of freedom," *Quantum Information Processing*, vol. 17, no. 11, p. 316, 2018.

[9] D. Shi, Y. Zhao, and J. Li, "Reconstructing part-level 3D models from a single image," in *Proceedings of the 2020 IEEE International Conference on Multimedia and Expo (ICME)*, vol. 42, pp. 65–79, IEEE, London, UK, July 2020.

[10] M. H. Anisi, A. H. Abdullah, S. A. Razak, and M. A. Ngadi, "Overview of data routing approaches for wireless sensor networks," *Sensors*, vol. 12, no. 4, pp. 3964–3996, 2012.

[11] F. Bajaber and I. Awan, "An efficient cluster-based communication protocol for wireless sensor networks," *Telecommunication Systems*, vol. 55, no. 3, pp. 387–401, 2014.

[12] F Ahmed, J. Batle, M. Elhoseny et al., "Robust general N user authentication scheme in a centralized quantum communication network via generalized GHZ states," *Frontiers of Physics*, vol. 13, no. 2, Article ID 130306, 2018.

[13] Y. Li, N. Yu, W. Zhang, W Zhao, X You, and M Daneshmand, "Enhancing the performance of LEACH protocol in wireless sensor networks," in *Proceedings of the*, pp. 16–21, Shanghai, April 2011.

[14] J. Yick, A. Bharathidasan, G. Pasternack, B. Mukherjee, and D. Ghosal, "Optimizing placement of beacons and data loggers in a sensor network - a case study," in *Proceedings of the 2004 IEEE Wireless Communications and Networking Conference, WCNC*, pp. 2486–2491, Atlanta, GA, USA, March 2004.

[15] K. S. Ahn, D. G. Kim, and B. S. Sim, "Balanced chain-based routing protocol(BCBRP) for energy efficient wireless sensor networks," in *Proceedings of the 9th IEEE International Symposium on Parallel and Distributed Processing with Applications Workshops*, pp. 12–21, Busan, Korea (South), May 2011.

[16] J. Yang, Y. Zhao, J. Liu et al., "No reference quality assessment for screen content images using stacked autoencoders in pictorial and textual regions," *IEEE Transactions on Cybernetics*, vol. 6, pp. 3–12, 2020.

[17] N. Zhaoyang, R. Yongxin, R. Chengao, and W. Xuehong, "ANSYS application in design of the main beam of crane," *Machinery for Lifting and Transportation*, vol. 5, pp. 31–33, 2008.

[18] G. P. Gupta, M. Misra, and K. Garg, "Towards scalable and load-balanced mobile agents-based data aggregation for wireless sensor networks," *Computers & Electrical Engineering*, vol. 64, no. 10, pp. 262–276, 2017.

[19] A. F. Metwaly, M. Z. Rashad, F. A. Omara, and A. A. Megahed, "Architecture of multicast centralized key management scheme using quantum key distribution and classical symmetric encryption," *The European Physical Journal - Special Topics*, vol. 223, no. 8, pp. 1711–1728, 2014.